ACS Sustainable Chemistry & Engineering

Research Article

pubs.acs.org/journal/ascecg

Improving Energy Conversion Efficiency of Dye-Sensitized Solar Cells by Modifying TiO_2 Photoanodes with Nitrogen-Reduced Graphene Oxide

Zhonghua Xiang, Xing Zhou, Gang Wan, Guoxin Zhang, and Dapeng Cao*

State Key Lab of Organic−Inorganic Composites, Beijing University of Chemical Technology, Beijing 100029, P.R. China

ABSTRACT: As potential third generation photovoltaic cells, dye-sensitized solar cells (DSSCs) have attracted extensive research interests and have become one of the hot topics in current research. In this work, a series of DSSCs based on TiO_2 photoanodes modified by graphene oxide (GO) and nitrogen-reduced graphene oxide (N-rGO) were fabricated. Results indicate that N-rGO is a better TiO_2 photoanode modifier of DSSCs compared to GO. With an increase in the amount of N-rGO, the open circuit voltage increases, while both the short circuit current and power conversion efficiency (PCE) of the DSSCs exhibit a maximum at the content of 0.2 wt % N-rGO. In particular, the maximum PCE of the DSSCs reaches 7.19% in this work, which gains a 13.23% enhancement compared to the PCE of 6.42% of conventional TiO_2 DSSCs. The enhancement of the PCE of the DSSCs with N-rGO was mainly attributed to the reduction in electron recombination and the increase in electron transfer efficiency after incorporating N-rGO into TiO_2 photoanodes.

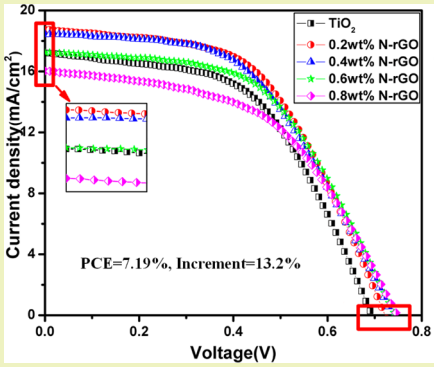

KEYWORDS: *Dye-sensitized solar cells, Nitrogen-doped graphene, Short circuit current, Open circuit voltage, Photovoltaic cells*

INTRODUCTION

Since the pioneering work on dye-sensitized solar cells (DSSCs) was reported by Gratzel and O'Regan in 1991,[1] DSSCs have attracted extensive research interests all over the world. In past decades, the preparation methods and assembly techniques of the DSSC have gained great breakthroughs. Currently, the power conversion efficiency (PCE) record of the DSSCs has reached 12.3%,[2] which indicates that the DSSCs are very likely to become third generation photovoltaic cells and will definitely challenge the dominance of the silicon cells in photovoltaic fields.

As the main component of DSSCs, photoanodes have been widely studied and prepared often by coating a semiconductor on conductive glass. The semiconductors act as not only a carrier to adsorb dyes by their large surface area but also an electron transformer owing to their unique nanostructures. Semiconductors used in the DSSCs usually include TiO_2, ZnO, Nb_2O_5, SnO_2,[3] and so on. Among these materials, TiO_2 has become the priority choice for its low cost, nontoxicity, and excellent photochemical stability up to now.[4] Recently, the methods attempting to incorporate foreign elements into conventional TiO_2 photoanodes were widely adopted to modify photoanodes, aiming at enlarging the light-harvesting, reducing recombination and promoting electron transfer. Hu et al.[5] optimized the DSSCs by designing TiO_2 photoanodes with three different layers including small pore size films, larger pore size films, and light-scattering particles. Their results show that DSSCs with optimized microstructures had better light-scattering effects, gaining a higher PCE compared to conventional DSSCs. In order to reduce the recombination between electron and oxidized dye as well as I_3^- in the electrolyte, Mane et al.[6] prepared a core−shell structure by using the layer-by-layer deposition to coat a 30 nm ZnO layer on TiO_2 film, in which the ZnO layer acts as an energy barrier to block electron transportation out of TiO_2, thereby reducing the recombination and leading to an increase in PCE from 3.31% to 4.51%. Recently, Bai et al.[7] reported a new type of photoanode architecture to promote electron transfer. The photoanode was prepared by *in situ* direct growth of ZnO nanowires within a TiO_2 nanoparticle film through a hydrothermal process, and the results show that an optimal amount of ZnO embedded in TiO_2 can enhance the PCE remarkably from 6.65% to 8.44%.

Graphene is a two dimensional honeycomb-like nanocrystal composed by sp^2 hybridized carbons, and it shows a spectacular conductivity at room temperature. The electron mobility reaches 15,000 $cm^2\ V^{-1}\ s^{-1}$,[8] which is much faster than ZnO (200−1000 $cm^2\ V^{-1}\ s^{-1}$) and TiO_2 (0.1−4 $cm^2\ V^{-1}\ s^{-1}$). Besides, graphene also exhibits the smallest resistance among all the substances on earth.[9] Recent researches show graphene provides the opportunity to enhance photovoltaic and electronic performance of the devices.[10−21] Fang et al.[22] incorporated graphene oxide (GO) into TiO_2 photoanodes and discovered that graphene can inhibit the charge recombination and increase the short circuit current (J_{sc}) to some extent, thus improving the PCE of the DSSCs. Recently, Dai's group[23] prepared a nitrogen-doped reduced graphene

Received: February 4, 2014
Revised: March 27, 2014
Published: April 1, 2014

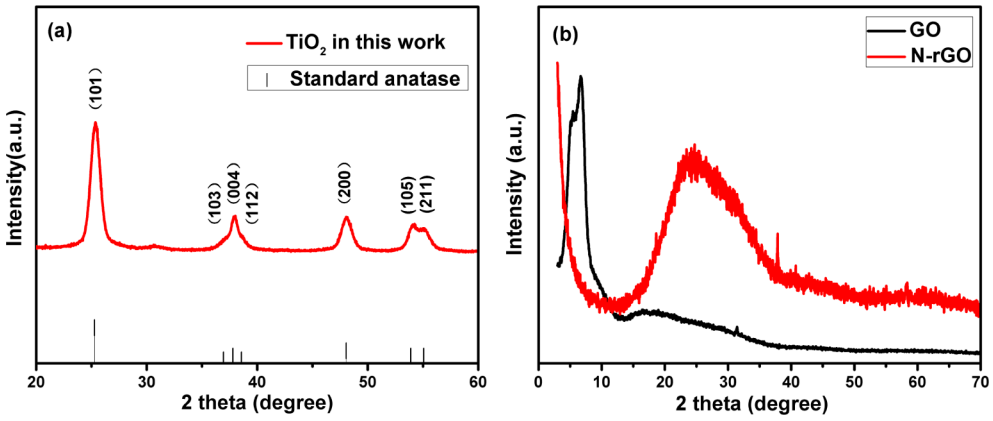

Figure 1. XRD patterns of (a) anatase TiO_2 and (b) GO and N-rGO.

oxide (N-rGO) foam for the counter electrode of DSSCs and discovered that the PCE of the DSSCs with N-rGO as a counter electrode material outperforms those with GO. However, the effect of incorporation of N-rGO in photoanodes on the PCE of DSSCs is rarely investigated. In this work, a series of photoanodes incorporated with different amounts of N-rGO were fabricated, and the PCEs of the corresponding DSSCs were investigated. For comparison, the PCE of DSSCs based on the photoanodes with different amounts of GO were also explored.

EXPERIMENTAL SECTION

Preparation of TiO_2 Slurry. The TiO_2 slurry was prepared by a hydrothermal method.[24] First of all, 1.5 g of acetic acid was added into 8.5 g of tetrabutyl titanate and stirred about 20 min at room temperature. Then, the mixture was poured into 50 mL of water as quickly as possible with vigorously stirring for 1 h. After 1 mL of concentrated nitric acid was added into the as-obtained white precipitate, the solution became aqua transparent. The precursor was heated to 80 °C within 40 min and peptized for 75 min. Then the mixture was treated by hydrothermal techniques under 200 °C for 16 h. After the autoclave cooling to room temperature, the upper solution was removed. Then, 0.6 mL of concentrated nitric acid and 30 mL of ethanol were added into the autoclave. The solution was ultrasonicated for 30 min, and the resulting solution was centrifuged and washed by ethanol three times. Following this step, 10 g of 10 wt % ethyl cellulose in ethanol solution, 8.1 g of terpineol, and another 30 mL of ethanol were added. After ultrasonic dispersion for another 30 min, the solution was concentrated with a rotary-evaporator. Finally, the slurry obtained contains 18% TiO_2, 9% ethyl cellulose, and 73% terpineol.

Preparation of GO and N-rGO. The GO was synthesized by a modified Hummers method.[25] Natural graphite (1 g, 50 mesh) was added into a 250 mL round-bottomed flask with 108 mL of concentrated sulfuric acid and 26 mL of concentrated phosphoric acid. The flask was placed in an ice bath, and 3g of $KMnO_4$ was slowly added while the temperature was kept below 20 °C for 1.5 h. The solution was then placed in an oil bath and heated at 35−40 °C for 1 h. Temperature was increased to 70 °C and kept for 30 min. Then, 10 mL of deionized water was added to the flask, where the temperature was increased to 100 °C and kept at that temperature for 20 min. After 20 min, another 10 mL of deionized water was added. After 30 min, 50 mL of deionized water was added. Then, 100 mL of ice deionized water was added to the resultant suspension, and this step diluted and cooled the system. After 15 min, 10 mL of 30% H_2O_2 was added to the flask under vigorous stirring. This suspension was stirred for 1 h at room temperature. The suspension was centrifuged at low speed three times (4500 rpm,15 min) and washed with a 5% HCl solution two times and then centrifuged at high speed three times (12,000 rpm, 60 m in) with distilled water (first step is to add 0.1 g of NH4Cl).

N-rGO was synthesized by solvothermal reduction.[26] A total of 10 mL of 0.2 mg/mL GO aqueous solution was dispersed for 30 min. Then, 2 mL of concentrated ammonia was added. After dispersion for another 30 min, the solution was transferred to a Teflon-lined autoclave and heated at 120 °C for 6 h.

Fabrication of DSSC. GO and N-rGO were added into terpineol to obtain 1 mL/mg solution. Then, the solution was dispersed for 30 min. In order to prepare different photoanodes, different amounts (0.05, 0.1, 0.15, and 0.2 mL) of GO and N-rGO dispersion were added in the mortar to mix with pure TiO_2 slurry to obtain 0.2, 0.4, 0.6, and 0.8 wt % GO and 0.2, 0.4, 0.6, and 0.8 wt % N-rGO incorporated slurries. Fluorine-doped tin oxide (FTO) conductive glass (NSG, 15Ω cm^{-2}) was cleaned with detergent, dilute HCl aqueous solution, and deionized water in an ultrasonic cleaner. Then, the slurries were made into films on FTO by a doctor-blade method. After being dried, the films were annealed at 450 °C for 60 min in air. The resulting electrode was immersed into a N3 ethanol solution for 24 h to form the sensitized photoanode. The counter electrode was Pt-coated film by thermal decomposition of platinochloric acid. The photoanodes and counter electrodes were assembled into sandwich-like cells with electrolytes composed of 0.05 M LiI, 0.05 M I_2, and 0.5 M *tert*-butylpyridine in solvent of acetonitrile.

Characterization of Different GO and N-rGO Incorporated Photoanodes. The current density−voltage (J−V) characteristics of DSSCs were measured under AM 1.5 simulated illumination (CHF-XM500, TRUSTTECH, Beijing) with a power density of 100 mW/cm^2 at an active area of 0.3 cm^2. Electrochemical impedance spectra (EIS) was conducted on CHI760E (CHINSTR, Shanghai) with a frequency range from 100 kHz to 0.1 Hz in the condition of open circuit under 100 mW/cm^2 irradiation. XPS measurements were performed using an ESCALAB 250 instrument (THERMO SCIENTIFIC, China) with Al Kα radiation. Powder X-ray diffraction measurements (PXRD) were performed by a D/MAX 2000 X-ray diffactometer (RIGAKU, Japan) with a Cu Kα line (λ = 1.54178 Å) as the incident beam. Scanning electron microscopy images were obtained on a S4700 SEM instrument (HITACHI, Japan). Transmission electron microscopy images were obtained on a JEM-3010 high-resolution TEM instrument (HITACHI, Japan). UV−visible absorption spectra were recorded on a UV−vis spectrometer (TU-1901, PERSEE, Beijing).

RESULTS AND DISCUSSION

Figure 1 shows the PXRD patterns of TiO_2, GO, and N-rGO. It is observed from Figure 1a that the peaks from the TiO_2 synthesized by the hydrothermal method are in excellent agreement with the standard anatase TiO_2. The anatase characteristic peak (1 0 1) was quite obvious, while no rutile characteristic peak (1 1 0) appears. As is well known, anatase has a wider band gap and higher energy level that makes anatase a better choice for DSSCs rather than rutile.[27]

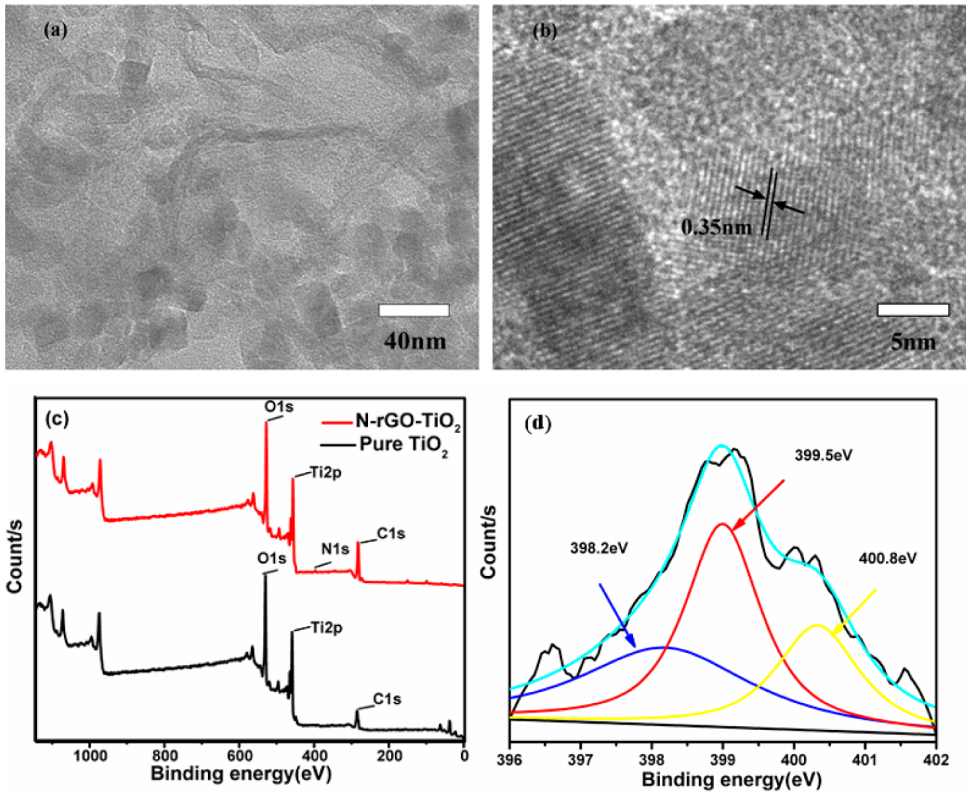

Figure 2. (a) TEM images of N-rGO incorporated TiO_2. (b) Magnified TEM images. (c) XPS spectra of the photoanodes with and without N-rGO. (d) High-resolution N 1s spectra of the N-rGO-TiO_2 photoanode. It (black) can be deconvoluted into three subpeaks: pyridinic nitrogen (398.2 eV; blue), pyrrolic nitrogen (399.5 eV; red), and graphitic nitrogen (400.8 eV; yellow). The cyan line refers to the fitted result.

According to the PXRD pattern, we used the Scherrer equation to predict that the average particle diameter was 21.65 nm, which is in good agreement with the one from the SEM images. Figure 1b shows that GO only had a very sharp peak at about 9°, which indicated that graphite (characteristic peak at about 26°) had been successfully oxidized to GO, and after reduction, the sample had a wide peak around 26°. The shift of peak suggested that GO had been partly reduced to N-rGO, and N-rGO had smaller interlayer spacing because of partly removing the oxygen-containing groups according to the Bragg eq $2d = \sin \theta$.

Figure 2a shows the TEM images of the TiO_2 film incorporated with N-rGO, which revealed that N-rGO was incorporated into the TiO_2 film and mixed with a large number of TiO_2 nanoparticles. No apparent aggregation was observed on the TEM image, which indicated that the TiO_2 nanoparticles could disperse uniformly on or between the N-rGO. The magnified TEM image (Figure 2b) displays the well-defined lattice fingers of TiO_2 nanoparticles, corresponding to the (1 0 1) plane of anatase TiO_2. The XPS spectra of the photoanodes with and without N-rGO are shown in Figure 2c, in which one N 1s peak appears in the N-rGO-incorporated photoanode. Furthermore, the C 1s peak in the N-rGO-incorporated photoanode becomes stronger than that in the pure TiO_2 photoanode. That is to say, the XPS spectra further confirmed that the N-rGO was successfully introduced into the photoanodes. As shown in the high resolution spectra of N 1s in Figure 2d, it can be deconvoluted into three subpeaks: pyridinic nitrogen (398.2 eV), pyrrolic nitrogen (399.5 eV), and graphitic nitrogen (400.8 eV).

The effects of incorporation of GO and N-rGO on the photocurrent, voltage, fill factor, and PCE of the TiO_2-based DSSCs were evaluated and are listed in Tables 1 and 2. The

Table 1. *J*–*V* Parameters of Different Amounts of GO Added

additions	V_{oc} (V)	J_{sc} (mA/cm2)	FF (%)	PCE (%)
TiO_2	0.693	17.10	54.18	6.40
0.2 wt % (0.05 mg) GO	0.723	17.32	54.02	6.77
0.4 wt % (0.10 mg) GO	0.727	17.11	53.21	6.62
0.6 wt % (0.15 mg) GO	0.734	16.61	53.08	6.48
0.8 wt % (0.20 mg) GO	0.739	16.01	51.25	6.05

Table 2. *J*–*V* Parameters of Different Amounts of N-rGO Added

additions	V_{oc} (V)	J_{sc} (mA/cm^2)	FF (%)	PCE (%)
TiO_2	0.695	17.19	53.14	6.35
0.2 wt % (0.05 mg) N-rGO	0.722	18.74	53.08	7.19
0.4 wt % (0.10 mg) N-rGO	0.739	18.42	52.64	6.94
0.6 wt % (0.15 mg) N-rGO	0.743	17.24	53.44	6.85
0.8 wt % (0.20 mg) N-rGO	0.748	16.11	51.04	6.12

measured *J*–*V* curves are shown in Figure 3a and b. It is observed from Tables 1 and 2 that when the content of GO or N-rGO is 0.05 mg, the PCE of DSSCs increases to the maximum value. In addition, our results show that when the same content of GO or N-rGO was incorporated into the photoanodes, N-rGO incorporation exhibits a better enhancement of PCE compared to GO incorporation. The corresponding PCEs of the DSSCs incorporated with 0.05 mg of N-rGO

dx.doi.org/10.1021/sc5000732 | ACS Sustainable Chem. Eng. 2014, 2, 1234−1240

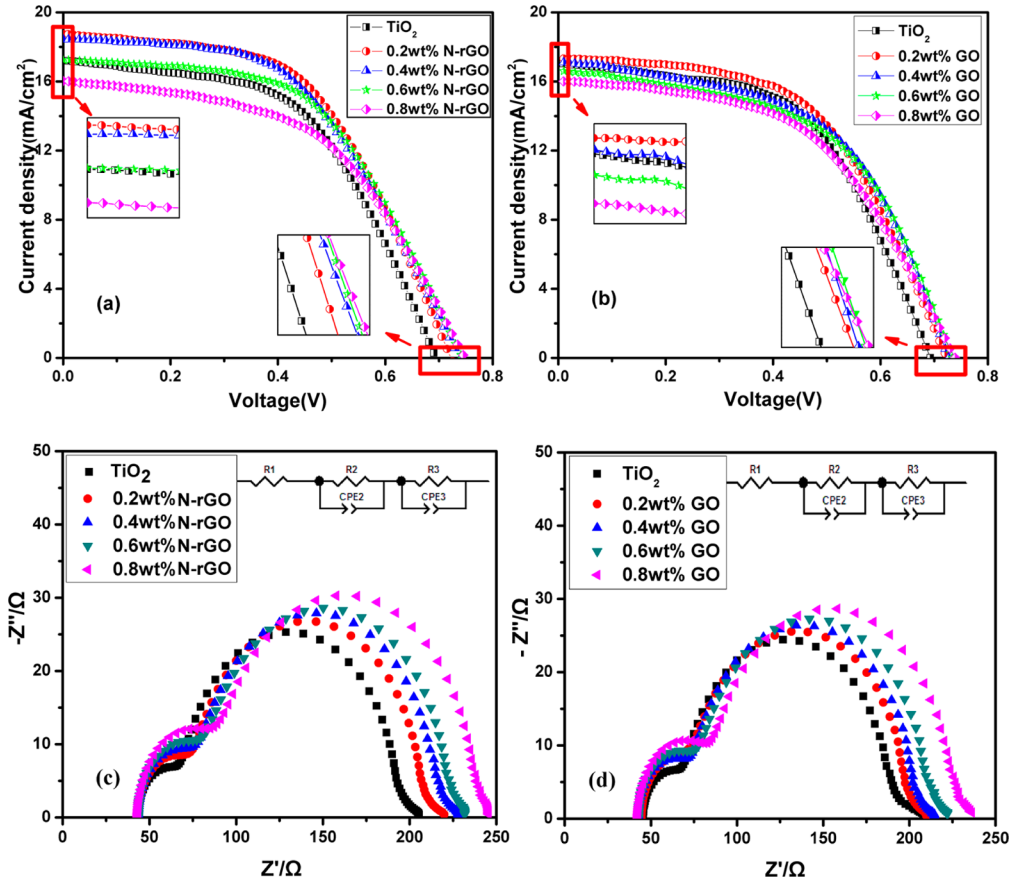

Figure 3. *J*−*V* curves of DSSCs with different electrodes: (a) with N-rGO and (b) with GO. EIS measurement of DSSCs with different electrodes: (c) with N-rGO and (b) with GO.

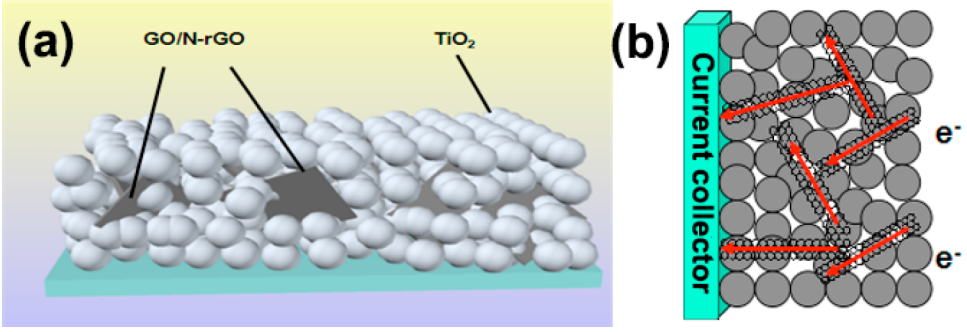

Figure 4. (a) Illustrations of the photoanode with N-rGO. (b) Electron transfer in the photoanode with N-rGO.

and GO are 7.19% and 6.77%, respectively, which increased by 13.23% and 5.78%, respectively, compared to pure TiO_2 DSSCs.

It should be noted that the PCE of DSSCs is affected significantly by the open circuit voltage (V_{oc}) and the short circuit current (J_{sc}). According to previous reports,[28,29] J_{sc} would be affected by the electron transfer efficiency, light scattering, and the dye absorption, while the V_{oc} would be mainly associated with the difference between the Fermi Level in the semiconductor and the Nernst potential of the redox couple. As shown in the inset of Figure 3a and b, V_{oc} increases with the content of GO and N-rGO. Ohsaki's research indicated that the lifetime of electrons in nanotubes is three times longer than in nanoparticles.[30] Because the graphene has a similar structure with the nanotubes, it can be inferred that the lifetime of electrons in graphene would also be longer than that in nanoparticles. Moreover, the electron mobility rates in the GO and N-rGO structure are extremely high. Therefore, the incorporation of GO and N-rGO could reduce the electron recombination to some extent, which was also proved by the EIS results. There are three semicircles in the EIS spectra theoretically. The high-frequency semicircle is attributed to the charge transfer at the counter electrode, while the response in the intermediate frequency region is associated with the electron transport in the TiO_2 film and the back reaction at the TiO_2/electrolyte interface. The low-frequency region reflects the electron diffusion in the electrolyte.[31] Obviously, it can be found from Figure 3c and d that the diameter of the second semicircle became bigger with the increase in content of GO and N-rGO. It indicates that the resistance of the electron

dx.doi.org/10.1021/sc5000732 | ACS Sustainable Chem. Eng. 2014, 2, 1234−1240

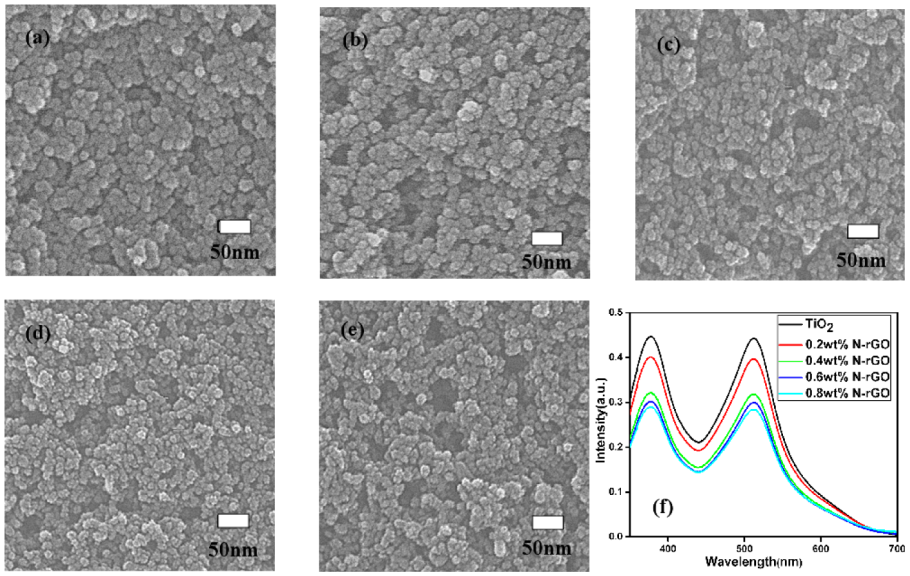

Figure 5. SEM images of photoanode films with different amounts of N-rGO: (a) 0 mg, (b) 0.05 mg, (c) 0.1 mg, (d) 0.15 mg, and (e) 0.2 mg. (f) Absorption spectra of the dye desorbed from above five films with an area of 2.0 cm^2 in 0.1 M NaOH solution (1:1 ethanol and deionized water).

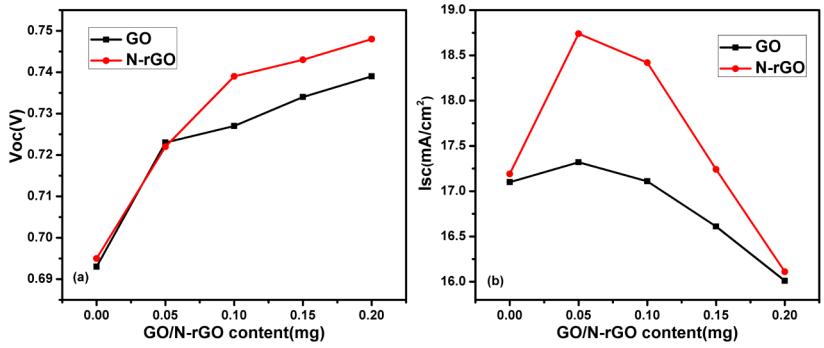

Figure 6. Trends of (a) V_{oc} and (b) J_{sc} with different contents of N-rGO and GO.

transfer at the TiO_2/dye/electrolyte interfaces becomes larger, meaning less electron recombination. Moreover, less recombination definitely means more electron density, and it would cause a slight shift of the Fermi level,[32] leading to an increase in V_{oc}.

Unlike V_{oc}, the J_{sc} is influenced by the electron transfer efficiency, light scattering, and dye adsorption simultaneously. It is shown in Figure 3a and b that J_{sc} first increases to the maximum value and then decreases. This observation can be explained by the synergistic effects of three factors on J_{sc}. First, the remarkable electrical transport property and well-defined 2D structures of GO or N-rGO indicate that they are good electron conductors, which is beneficial to capture and transport electrons generated from TiO_2 irradiated by light to the GO or N-rGo network (Figure 4).[17,33] That is to say, the GO or N-rGO would act as a bridge to speed up electron transportation to electron collector (Figure 4b), leading to a decrease in the preferable electron−hole recombination in the pristine TiO_2 photoanode.[33] Therefore, incorporation of GO and N-rGO would increase the electron transfer efficiency in the TiO_2 nanostructure. Second, with an increase in GO and N-rGO, the porosity of the nanostructure would increase gradually, as observed from the SEM image in Figure 5. However, the optimal porosity for the photoanode was considered to be between 50% and 60%.[34] Too many pores would destruct the compact structure of the film and even lead to a crack in the surface of the film. It can be proven by a dye adsorption measurement that the overfull increased porosity is fatal to the DSSCs. Figure 5f shows the UV−vis absorption spectra of the dye desorbed from photoanodes with different amounts of N-rGO. Clearly, the incorporation of GO and N-rGO leads to a decrease in dye adsorption, which is a disadvantage for DSSCs. Third, the 2D N-rGO can serve as light-scattering centers to form more porous structures,[35] which would be advantageous for light harvesting. On the basis of the above analysis, the synergistic effects of the three factors (electron transfer efficiency, light scattering, and dye adsorption) on J_{sc} lead us to conclude that J_{sc} exists as a maximum value.

It was quite obvious that N-rGO incorporation exhibits a better enhancement for the PCE of DSSCs compared to GO under the same additions. Figure 6 shows the changing trends of V_{oc} and J_{sc} caused by different contents of GO and N-rGO incorporated. Apparently, the V_{oc} and J_{sc} yielded by N-rGO incorporation are always greater than those by GO incorporation, which further confirms the above analysis. This phenomenon can be explained by the doping of nitrogen. Compared to GO, N-rGO is better in improving the PCE of DSSCs as the photoanode modifier. This can be easily explained as follows. When the carbon atoms within the

graphene layers are substituted by nitrogen atoms in the form of graphitic nitrogen (a n-type element), the conductivity of N-rGO would increase remarkably,[36] and the excited elections are therefore transferred faster in the delocalized π structure in N-rGO-modified photoanodes than in GO-modified photoanodes.

CONCLUSIONS

We have investigated the effects of GO and N-rGO incorporations in TiO_2 on the PCE of the DSSCs. Results indicate that N-rGO is a better TiO_2 photoanode modifier of DSSCs compared to GO. With an increase in the N-rGO addition, the V_{oc} of the DSSCs increases because the incorporation of N-rGO can reduce the electron recombination, while the J_{sc} shows a maximum at the content of 0.2 wt % N-rGO owing to the synergistic effects of the electron transfer efficiency, light scattering, and dye adsorption after incorporating N-rGO. As a result, the PCE of the DSSCs also shows the same tendency as the short circuit current. In particular, the PCE of the DSSCs with 0.2 wt % N-rGO reaches 7.19%, which gains a 13.23% enhancement compared to the PCE of 6.42% of conventional TiO_2 DSSCs.

AUTHOR INFORMATION

Corresponding Author

*Fax: 86-10-64427616. Tel: +8610-64443254. Email: caodp@mail.buct.edu.cn.

Notes

The authors declare no competing financial interest.

ACKNOWLEDGMENTS

This work is supported by the National 863 Programs (2013AA031901), National NSF of China (91334203, 21274011), National Basic Research Program (2011CB706900), National Scientific Research Funding (ZZ1304), and Outstanding Talent Funding (RC1301) from BUCT.

REFERENCES

(1) O'regan, B.; Grätzel, M. A low-cost, high-efficiency solar cell based on dye-sensitized. *Nature* **1991**, *353*, 24.

(2) Yella, A.; Lee, H. W.; Tsao, H. N.; Yi, C. Y.; Chandiran, A. K.; Nazeeruddin, M. K.; Diau, E. W. G.; Yeh, C. Y.; Zakeeruddin, S. M.; Grätzel, M. Porphyrin-sensitized solar cells with cobalt (II/III)−based redox electrolyte exceed 12% efficiency. *Science* **2011**, *334*, 629−634.

(3) Chen, X. B.; Mao, S. S. Titanium dioxide nanomaterials: Synthesis, properties, modifications, and applications. *Chem. Rev.* **2007**, *107*, 2891−2959.

(4) Grätzel, M. Conversion of sunlight to electric power by nanocrystalline dye-sensitized solar cells. *J. Photochem. Photobiol., A* **2004**, *164*, 3−14.

(5) Hu, L. H.; Dai, S. Y.; Weng, J.; Xiao, S. F.; Sui, Y. F.; Huang, Y.; Chen, S.; Kong, F.; Pan, X.; Liang, L. Microstructure design of nanoporous TiO_2 photoelectrodes for dye-sensitized solar cell modules. *J. Phys. Chem. B* **2007**, *111*, 358−362.

(6) Mane, R. S.; Lee, W. J.; Pathan, H. M.; Han, S. H. Nanocrystalline TiO_2/ZnO thin films: Fabrication and application to dye-sensitized solar cells. *J. Phys. Chem. B* **2005**, *109*, 24254−24259.

(7) Bai, Y.; Yu, H.; Li, Z.; Amal, R.; Lu, G. Q. M.; Wang, L. In situ growth of a ZnO nanowire network within a TiO_2 nanoparticle film for enhanced dye-sensitized solar cell performance. *Adv. Mater.* **2012**, *24*, 5850−5856.

(8) Stoller, M. D.; Park, S.; Zhu, Y. W.; An, J.; Ruoff, R. S. Graphene-based ultracapacitors. *Nano Lett.* **2008**, *8*, 3498−3502.

(9) Meyer, J. Carbon sheets an atom thick give rise to graphene dreams. *Science* **2009**, *324*, 875−877.

(10) Li, B.; Liu, T.; Wang, Y.; Wang, Z. ZnO/graphene-oxide nanocomposite with remarkably enhanced visible-light-driven photocatalytic performance. *J. Colloid Interface Sci.* **2012**, *377*, 114−121.

(11) Wang, W.; Yu, J.; Xiang, Q.; Cheng, B. Enhanced photocatalytic activity of hierarchical macro/mesoporous TiO_2−graphene composites for photodegradation of acetone in air. *Appl. Catal., B* **2012**, *119*−*120*, 109−116.

(12) Luo, Q.-P.; Yu, X.-Y.; Lei, B.-X.; Chen, H.-Y.; Kuang, D.-B.; Su, C.-Y. Reduced graphene oxide-hierarchical ZnO hollow sphere composites with enhanced photocurrent and photocatalytic activity. *J. Phys. Chem. C* **2012**, *116*, 8111−8117.

(13) Zhao, Z.; Zhang, G.; Sun, L.; Gao, Y.; Yang, X.; Li, Y. Synthesis of a hierarchical three-component nanocomposite structure system with enhanced electrocatalytic and photoelectrical properties. *Chem.—Eur. J.* **2012**, *18*, 5248−5255.

(14) Ma, C.; Shao, X.; Cao, D. P. Nitrogen-doped graphene nanosheets as anode materials for lithium ion batteries: A first-principles study. *J. Mater. Chem.* **2012**, *22*, 8911−8915.

(15) Xiang, Q.; Yu, J.; Jaroniec, M. Graphene-based semiconductor photocatalysts. *Chem. Soc. Rev.* **2012**, *41*, 782−796.

(16) Kim, H.-i.; Moon, G.-h.; Monllor-Satoca, D.; Park, Y.; Choi, W. Solar photoconversion using graphene/TiO_2 composites: Nanographene shell on TiO_2 core versus TiO_2 nanoparticles on graphene sheet. *J. Phys. Chem. C* **2011**, *116*, 1535−1543.

(17) Chen, C.; Cai, W.; Long, M.; Zhou, B.; Wu, Y.; Wu, D.; Feng, Y. Synthesis of visible-light responsive graphene oxide/TiO_2 composites with P/N heterojunction. *ACS Nano* **2010**, *4*, 6425−6432.

(18) Madhusudan, P.; Yu, J.; Wang, W.; Cheng, B.; Liu, G. Facile synthesis of novel hierarchical graphene-$Bi_2O_2CO_3$ composites with enhanced photocatalytic performance under visible light. *Dalton Trans.* **2012**, *41*, 14345−14353.

(19) Xiang, Z.; Cao, D. P.; Huang, L.; Shui, J.; Wang, M.; Dai, L. M. Nitrogen-doped holey graphitic carbon from 2D covalent organic polymers for oxygen reduction. *Adv. Mater.* **2014**, DOI: 10.1002/adma.201306328.

(20) Zhu, J.; Chen, M.; He, Q.; Shao, L.; Wei, S.; Guo, Z. An overview of the engineered graphene nanostructures and nanocomposites. *RSC Adv.* **2013**, *3*, 22790−22824.

(21) Su, X.; Wu, Q.; X, Z.; Wu, J.; Wei, S.; Guo, Z. Advanced titania nanostructures and composites for lithium ion battery. *J. Mater. Sci.* **2012**, *47*, 2519−2534.

(22) Fang, X. L.; Li, M. Y.; Guo, K. M.; Zhu, Y. D.; Hu, Z. Q.; Liu, X. L.; Chen, B.; Zhao, X. Improved properties of dye-sensitized solar cells by incorporation of graphene into the photoelectrodes. *Electrochim. Acta* **2012**, *65*, 174−178.

(23) Xue, Y.; Liu, J.; Chen, H.; Wang, R.; Li, D.; Qu, J.; Dai, L. Nitrogen-doped graphene foams as metal-free counter electrodes in high-performance dye-sensitized solar cells. *Angew. Chem., Int. Ed.* **2012**, *51*, 12124−12127.

(24) Ito, S.; Murakami, T. N.; Comte, P.; Liska, P.; Grätzel, C.; Nazeeruddin, M. K.; Grätzel, M. Fabrication of thin film dye sensitized solar cells with solar to electric power conversion efficiency over 10%. *Thin Solid Films* **2008**, *516*, 4613−4619.

(25) Huang, N. M.; Lim, H.; Chia, C.; Yarmo, M.; Muhamad, M. Simple room-temperature preparation of high-yield large-area graphene oxide. *Int. J. Nanomed.* **2011**, *6*, 3443.

(26) Wang, H. B.; Maiyalagan, T.; Wang, X. Review on recent progress in nitrogen-doped graphene: synthesis, characterization, and its potential applications. *ACS Catal.* **2012**, *2*, 781−794.

(27) Hagfeldt, A.; Boschloo, G.; Sun, L. C.; Kloo, L.; Pettersson, H. Dye-sensitized solar cells. *Chem. Rev.* **2010**, *110*, 6595−6663.

(28) Zhou, Y.; Chen, L.; Tu, W. G.; Bao, C. X.; Dai, H.; Tao, Y.; LIU, J.-g. Enhanced photovoltaic performance of dye-sensitized solar cell using graphene-TiO_2 photoanode prepared by a novel in situ simultaneous reduction-hydrolysis technique. *Nanoscale* **2013**, *5*, 3481−3485.

(29) Yang, N. L.; Zhai, J.; Wang, D.; Chen, Y. S.; Jiang, L. Two-dimensional graphene bridges enhanced photoinduced charge transport in dye-sensitized solar cells. *ACS Nano* **2010**, *4*, 887−894.

(30) Ohsaki, Y.; Masaki, N.; Kitamura, T.; Wada, Y.; Okamoto, T.; Sekino, T.; Niihara, K.; Yanagida, S. Dye-sensitized TiO_2 nanotube solar cells: Fabrication and electronic characterization. *Phys. Chem. Chem. Phys.* **2005**, *7*, 4157−4163.
(31) Wang, Q.; Moser, J. E.; Grätzel, M. Electrochemical impedance spectroscopic analysis of dye-sensitized solar cells. *J. Phys. Chem. B* **2005**, *109*, 14945−14953.
(32) Tan, B.; Wu, Y. Y. Dye-sensitized solar cells based on anatase TiO_2 nanoparticle/nanowire composites. *J. Phys. Chem. B* **2006**, *110*, 15932−15938.
(33) Ng, Y. H.; Lightcap, I. V.; Goodwin, K.; Matsumura, M.; Kamat, P. V. To what extent do graphene scaffolds improve the photovoltaic and photocatalytic response of TiO_2 nanostructured films? *J. Phys. Chem. Lett.* **2010**, *1*, 2222−2227.
(34) Kopidakis, N.; Benkstein, K. D.; van de Lagemaat, J.; Frank, A. J. Transport-limited recombination of photocarriers in dye-sensitized nanocrystalline TiO2 solar cells. *J. Phys. Chem. B* **2003**, *107*, 11307−11315.
(35) Koo, H. J.; Park, J.; Yoo, B.; Yoo, K.; Kim, K.; Park, N. G. Size-dependent scattering efficiency in dye-sensitized solar cell. *Inorg. Chim. Acta* **2008**, *361*, 677−683.
(36) Shao, Y. Y.; Zhang, S.; Engelhard, M. H.; Li, G. S.; Shao, G. C.; Wang, Y.; Liu, J.; Aksay, I. A.; Lin, Y. Nitrogen-doped graphene and its electrochemical applications. *J. Mater. Chem.*. **2010**, *20*, 7491−7496.